Available online at www.sciencedirect.com
SCIENCE DIRECT®
International Journal of Machine Tools & Manufacture 44 (2004) 785–796
INTERNATIONAL JOURNAL OF MACHINE TOOLS & MANUFACTURE DESIGN, RESEARCH AND APPLICATION
www.elsevier.com/locate/ijmactool

Effect of heat sink on microstructure of three-dimensional parts built by welding-based deposition

Z. Jandric, M. Labudovic, R. Kovacevic *

Research Center for Advanced Manufacturing (RCAM), Southern Methodist University, 1500 International Parkway, Suite 100, Richardson, TX 75081, USA

Received 2 January 2003; received in revised form 19 December 2003; accepted 15 January 2004

Abstract

This paper concentrates on the microstructural analysis of the three-dimensional (3D) parts built by rapid prototyping (RP) based on gas tungsten arc welding (GTAW). The material used for building 3D parts is AISI 1018. Two sets of experiments are carried out. From each experiment, samples are obtained by a standard metallographical procedure: cross sectioning, polishing, and etching. During the first experiment, the temperature at the locations with different heat-transfer conditions are monitored by thermocouples. The relationships between the geometry of the deposited beads and the welding parameters are developed. The microstructure analysis of fusion and the heat-affected zone is performed. Samples from the second experiment are examined on Vickers microhardness tests. The results showed that the deposited layers possess a maximum hardness at the top layer with a slight decrease towards the middle and bottom layers. The obtained results show that 3D parts built in this manner have a very uniform microstructure and are free of cracks and porosity.

Keywords: Rapid prototyping; GTAW; Volume of heat sink; Microstructure; Microhardness

1. Introduction

Market need has forced manufacturing companies to look for a technology that can make products directly from a 3D computer aided design (CAD) electronic file. In the last decade, it has been shown that RP through layered manufacturing principles is an attractive method for 3D object generation. Layered manufacturing technology is the key technology of the RP systems that allows for the fabrication of 3D parts layer by layer. The most common processes are stereolithography, laser-engineered net shaping (LENS), laminated object manufacturing, selective laser sintering (SLS), 3D cladding, 3D printing, and shape deposition manufacturing (SDM). Most of the RP systems still make parts from non-metallic materials while others systems that make metallic parts are making objects that are porous, have weak bonds between layers and, consequently, have structural weakness.

RP based on deposition by welding overcomes this disadvantage. Produced 3D parts are built from metal; they are dense and porous-free yet have very good metallurgical bonding between the layers. When this technique is combined with the CNC milling, manufactured parts are geometrically accurate and have a good surface appearance as well [1–3]. Several research-teams have shown that this technique is capable of making diverse part shapes [4–8].

The welding process for building 3D parts was mentioned for the first time in 1925 by R. Baker to produce receptacles or containers of ornamental and useful shapes. The first known application of RP based on deposition by welding was reported in Germany in the 1960s when several free-standing shapes were built. A number of researchers [9–13] have contributed in developing this process; although, they were mainly concerned with the equipment set-up and possible

* Corresponding author. Tel.: +1-214-768-4865.
E-mail address: kovacevi@engr.smu.edu (R. Kovacevic).

0890-6955/$ - see front matter © 2004 Elsevier Ltd. All rights reserved.
doi:10.1016/j.ijmachtools.2004.01.009

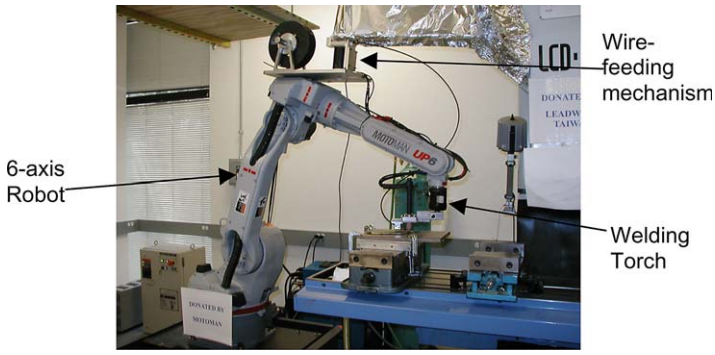

Fig. 1. New experimental set-up.

applications, and less with the quality of the produced parts or problems met in the process. The RP based on deposition by welding has been developed to fabricate various components of aircraft engines and pressure vessels in iron-based, nickel-based, and titanium-based alloys [4,14,15]. In this paper an iron-based alloy (AISI 1018) is used.

During the building of 3D parts with relatively complex geometry, it is noticed that even though the level of the heat input is kept constant, the size of the molten pool significantly alters. Namely, the size of the heat sink, which depends on the 3D geometry of already deposited material, plays a crucial role in this phenomenon [16–18]. The smaller the heat sink, the smaller amount of heat transferred through conduction, which means that a larger amount of energy is used for heating and melting of feeding and base material. For this reason, the molten pool enlarges when the heat source, optimized for obtaining a good depositional result on the locations that are remote from boundaries, is placed in the vicinity of the internal or external edges, corners and channels. The scientific challenge of RP based on deposition by welding is to control the dimensions and properties of the buildups. The control of the molten pool size and solidification time can offer both the desired dimension by limiting the molten pool size and the desired properties through microstructure manipulation. A stable and repeatable procedure of building layers is crucial for the quality of the fabricated part such as the geometrical accuracy, the level of residual stresses, the microstructure, the bonding, etc. To achieve this kind of the control, a better understanding is required of: the relationship between the independent process parameters and dimensions, the microstructure, and the properties. In this article, a feasibility study of RP based on deposition by gas tungsten arc welding has been performed. The relationship between the welding parameter settings, microstructure, and properties is investigated to obtain a better understating of the deposition process.

2. Experimental procedure

Experiments are carried out on the new experimental set-up, which is shown on Fig. 1. In this set-up, rapid prototyping based on deposition by welding uses gas tungsten arc welding (GTAW), and as a material, it uses an iron-carbon alloy (AISI 1018). To start the arc, a high voltage is used to break down the insulating gas between the non-consumable electrode and the workpiece. The electric arc is produced by a passage of current through the conductive ionized shielding gas. Current is then constantly transferred through the electrode to keep the electrode arc. Once the arc and weld pool are established, the torch is moved, and the arc progressively melts the substrate surface and filler metal (Fig. 2). Besides the equipment, the most important aspects of the GTAW process are the welding parameters. To achieve a specific weld quality and production output, suitable welding parameters must be used. The most influential parameters are welding current, arc voltage, wire feeding speed, welding speed, type and purity of the shielding gas, shielding gas flow rate, arc length, electrode tip geometry, and electrode material.

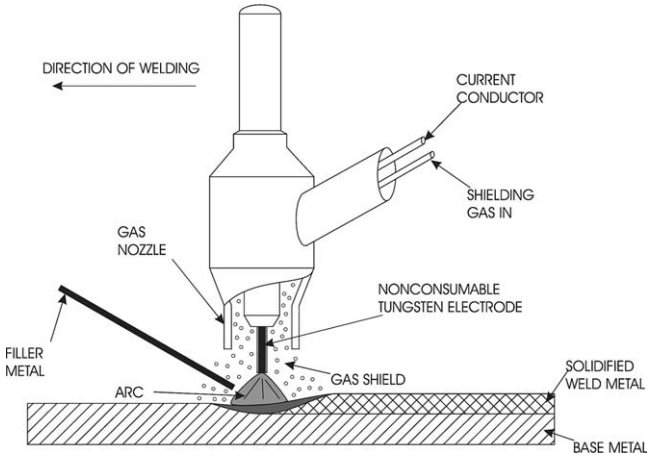

Fig. 2. Gas tungsten arc welding process.

In these experiments, a tungsten electrode 2.25 mm in diameter and pure argon as a shielding gas are applied. During the experiment, the distance between the tungsten electrode and the workpiece is held to be 2 mm. The travel speed of the welding torch is 3.81 mm/s, the diameter of the feed wire is 0.85 mm, and the flow of the shielding gas is 235 mm^3/s. The welding torch is positioned at the robot arm (see Fig. 1), and the tip of the electrode is used as a 'tool control point' during programming of the robot, so all parameters of motion are controlled through this point. A new wire-feeding mechanism is designed to provided the constant feeding speed of the wire during the deposition process, regardless of the robot's position (see Fig. 1). The wire-feeding mechanism is controlled by the stepping motor that is connected to the drive and further to the data acquisition board and a personal computer (PC)-based controller. The same controller controls the power supply and communicates with the robot's controller.

Two sets of experiments are performed. In the first experiment, a welding bead is deposited along the edges of the 3D part (Fig. 3), where the 3D part is designed so that the volume of heat sink, i.e. the surrounding mass of the material, varies between 12.5% and 100% of the maximum possible volume. The goal is to simulate different heat-transfer conditions and accordingly to establish a relationship between different heat transfer conditions, and bead geometry, and its microstructure. Experiment I is done for nine combinations of the welding current (80, 120, and 160 A), and the filler metal feeding speed (40, 80, and 120 cm/min). The second experiment (Fig. 4) is designed so that material is deposited in layers. The goal of the second experiment is to find which parameters produce a better layer. The quality of the layer is judged by verifying that the layer is crack-and-void-free, examining surface smoothness and determining the mechanical properties. Eighteen experiments are carried out with wire feeding speeds of 40, 80, and 120 cm/min, welding currents of 120 and 160 A, and for each combination of the wire-feeding speed and welding current, the material is deposited in one, two, and three layers. In every experiment, the wire-feeding speed and the heat input, i.e. the welding current, are kept constant.

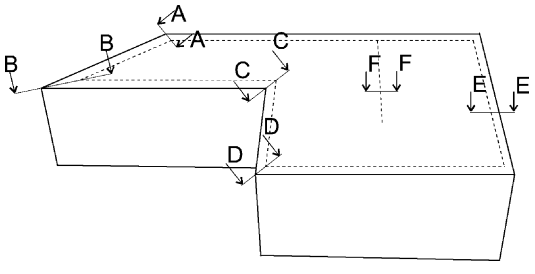

Fig. 3. Experiment I.

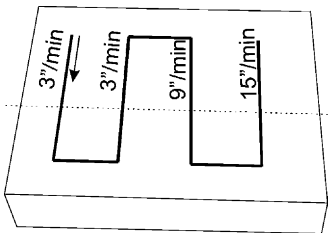

Fig. 4. Experiment II.

3. Results and discussion

3.1. Weld bead geometry and temperatures

After depositing beads, each sample is cross sectioned using an abrasive cut-off wheel, polished to a 1-μm finish, and etched in a 2% Nital solution. The workpiece from the first experiment is cut through the A–A, B–B, C–C, D–D, E–E, and F–F cross sections (see Fig. 3) in order to obtain information about the weld-bead geometry and microstructure at critical angles; while for the second experiment, the location of the cross-sections is irrelevant. A few images of the weld bead cross sections from the first experiment for the wire-feeding speed of 40 cm/min and for the welding currents of 80, 120, and 160 A, are shown in Table 1. The individual cross-sectional areas of the melted substrate and deposited filler metal are then measured. Figs. 5a–c present the mean values of the bead widths, the depths of the penetration, and the height of bead build-ups as the function of the bead location, i.e. the angle that is equivalent to the size of volume of the heat sink. The larger the angle the larger the volume of the heat sink. Experimental data of the bead width are approximated with a second-order function, while the experimental data for the bead width and depth of penetration are approximated with linear functions. It is interesting to note that while the bead width and depth of penetration decrease with an increase in the volume of the heat sink from 45° to 360°, 2.15 and 2.06 times, respectively, the underlying geometry basically has no influence on the height of the build-ups. Although the experimental data fluctuate, a strong influence of the bead location on the welding results is evident.

It is expected that different heat-transfer conditions will cause different temperature distribution within the workpiece. To check how much the bead location (different angles) will alter the temperature, k-type thermocouples are employed. To avoid eventual over-melting of the workpiece which can result in possible damage to the embedded thermocouples, and consequently incorrect readings, the next procedure is followed. For each thermocouple, a hole is drilled vertically from the bottom of the sample. The depth of the each hole is

Table 1
Cross-sections of the bead for the different geometrical factors

v_f [cm/min]	I [A]		
	80-40	120-40	160-40
0.125 (45°)	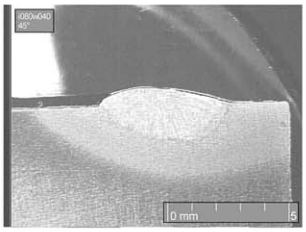	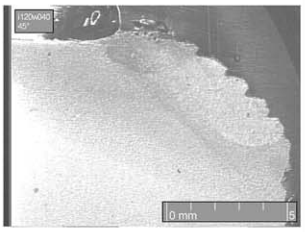	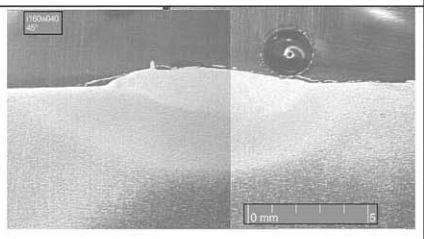
0.25 (90°)	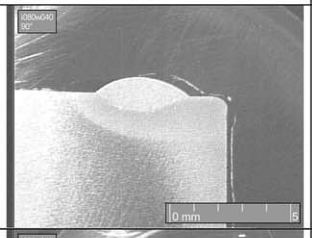	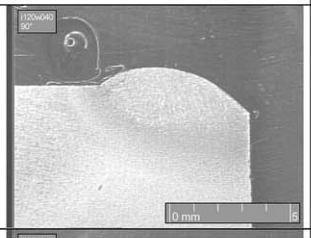	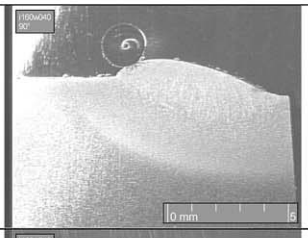
0.375 (135°)	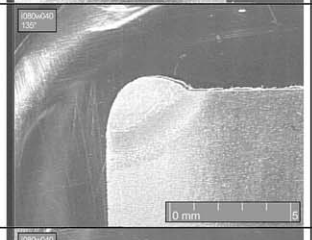	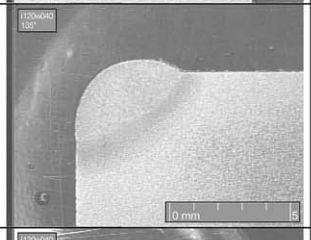	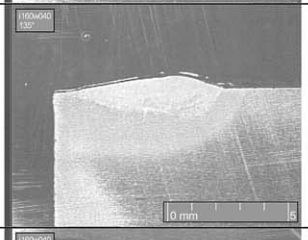
0.5 (180°)	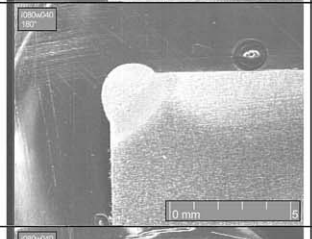	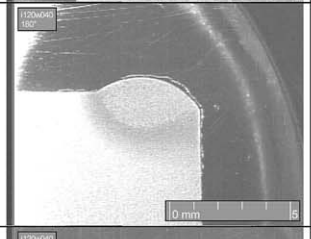	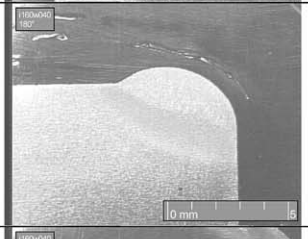
0.75 (270°)	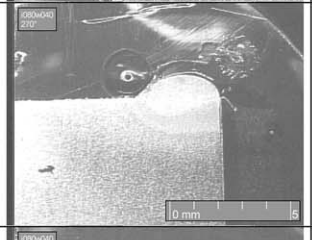	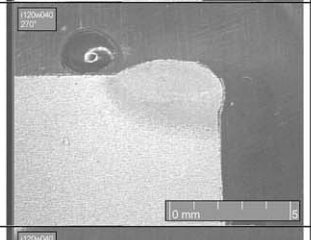	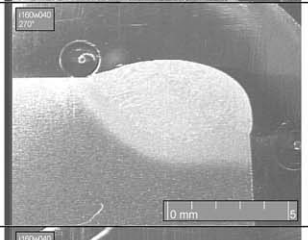
1 (360°)	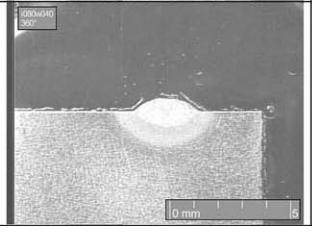	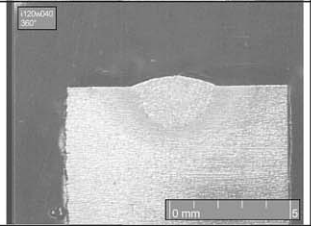	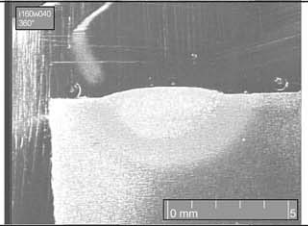

2 mm less than the height of the sample. From Fig. 5b, it can be seen that the largest depth of penetration is less than 2 mm, which means that thermocouples are placed in the heat affected zone (HAZ) where melting does not occur and where temperatures are within the range of thermocouple readings. To isolate thermocouples from a noise that originates from the arc, in the bottom of the each hole thermally conductive and electrically insulating high temperature cement is placed. The thermocouples and thermally conductive

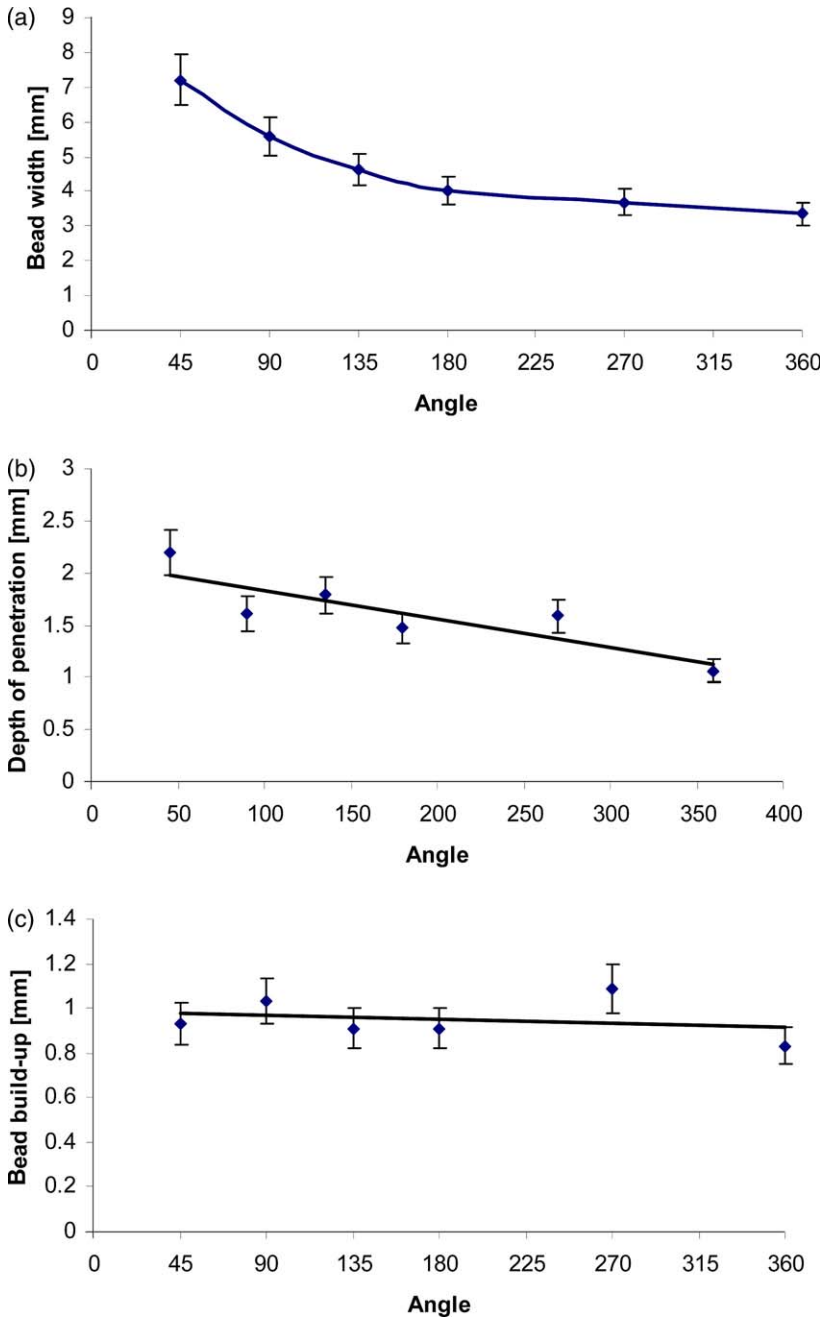

Fig. 5. (a–c) Influence of the geometry on the bead. (a), Bead width; (b), depth of penetration; (c) bead build-up.

cement are inserted together and left for the cement to cure (Fig. 6).

Recordings from the thermocouples are shown in Fig. 7. As it can be seen from the figure, different temperature histories are recorded for different angles. Logically, the highest temperature is achieved where the volume of the heat sink is the smallest—at an angle of 45°. As the angle increases, more material conducts the heat, and a smaller temperature is reached. It should be noted that ten readings are recorded per second; thus, 10 units at the horizontal axis represent one second. It can be seen that the workpiece is first preheated to approximately 100 °C by striking the arc, setting the welding current on 40 A, and moving the torch above the workpiece, then is let about 20 s to achieve uniform temperature (so that initial conditions are the same). Then, the arc is struck again, and the material is deposited along the edges. As soon the arc is positioned in the vicinity of the thermocouple, the temperature is increased fast, and the curve is very steep. After reaching the maximum temperature, the workpiece cools down fast, to about 300 °C. However,

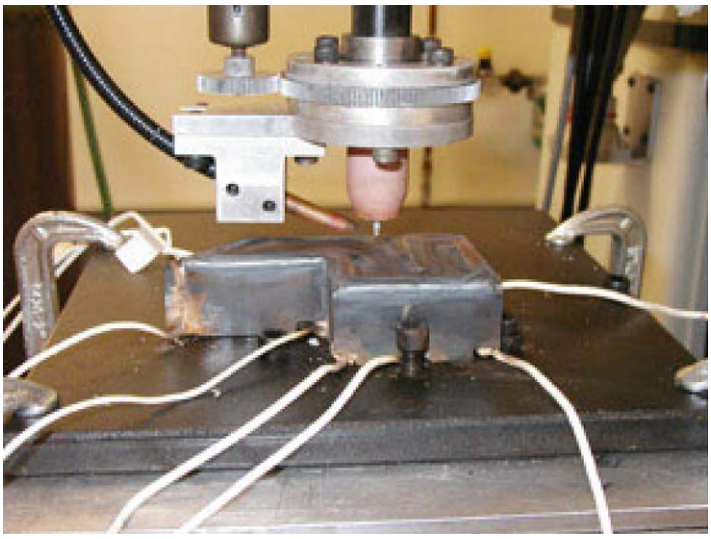

Fig. 6. Embedded thermocouples.

the cooling speed is different for different angles (see Fig. 7). The smaller the volume of the heat sink, the higher temperature reached, and the faster the cooling speed. This phenomenon will greatly affect the microstructure of the bead.

Since the torch path is a closed curve (see Fig. 3), there is also a small influence of the heat conducted from the other side of the body. For this reason, the temperature history curves have an irregular 'wavy' shape. The whole experiment last about 80 seconds; then the arc is turned off. It can be noticed from Fig. 7 that soon after the experiment, the temperatures of the body at the different points converge to approximately the same temperature. In Fig. 8 is shown relationship between the highest achieved temperatures and the angles. The overall difference in temperatures of ~250 °C within HAZ is not negligible since this difference can only be higher within the melted metal, and its significance will be evident when the microstructure is taken into consideration in the following paragraphs.

3.2. Microstructural analysis

The material used in this experiment is plain carbon steel, AISI 1018, with a chemical composition shown in Table 2. Since the mechanical properties of materials depend on their microstructure, the distribution and the nature of the phases within the microstructure, the process parameters have to be controlled so that a desired microstructure is achieved. By changing the process parameters, the temperature gradient (G) and the solidification rate (R) are altered. Therefore, in the case of welding, the array of microstructures and thus mechanical properties can be obtained. In the case of low-carbon steels, the final microstructure depends on the austenite-to-ferrite transformation when steel is cooled to an ambient temperature.

The microstructure of the original material is shown in Fig. 9. It is initially at an ambient temperature and has a microstructure that depends upon its past thermo-mechanical history. It is comprised of a mixture

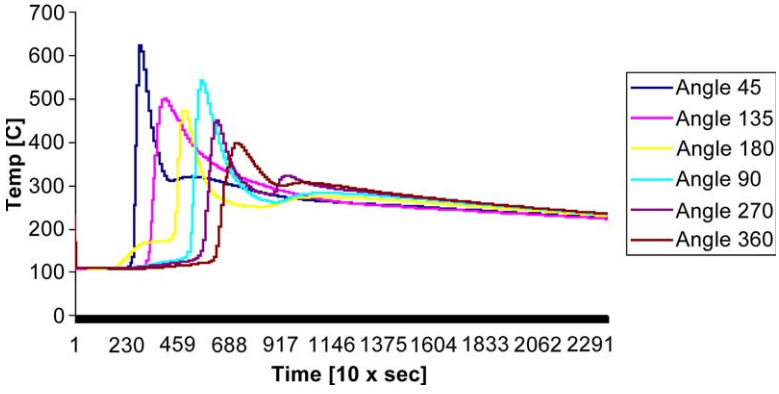

Fig. 7. Recordings from the thermocouples.

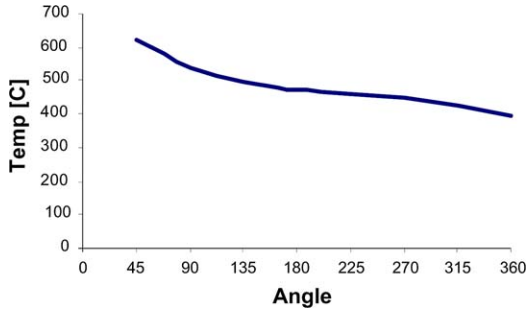

Fig. 8. Temperature drop with the angle of the workpiece.

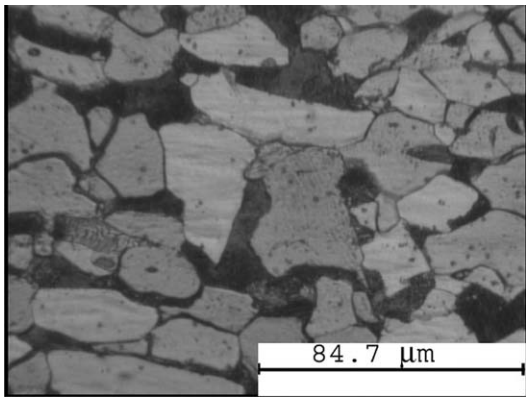

Fig. 9. Original material.

of cementite and ferrite. There are free ferrite grains, and regions of pearlite in which the two phases exist as a lamellar mixture. In Fig. 9, the lamellar pearlite is represented with dark regions and ferrite with light regions. On top of this original material is deposited the welding bead; thus, a portion of the original material is melted together with filler metal, and a portion of it is exposed to a sufficient temperature that will cause a recrystallization but not melting. So, each bead consists of the melted zone (marked as I in Fig. 10a–c) and the heat affected zone (HAZ) (marked as II in Fig. 10a–c). The melted zone of the bead (the upper part) consists of the build-up and depth of penetration. From Fig. 10a–c, it is obvious that the overall length of the beads is different. The longest bead is the one at 45°, which is the smallest observed volume of the heat sink, while the shortest is at 360°. Logically, the longest bead has the longest melted as well as heat affected zone. This result is a direct consequence of the highest temperature that this section of the part is exposed to. Since the heat transfer conditions are much more different at 45° and 270° than at 270° and 360°, the beads at 270° and 360° are more alike.

Also from these images, the size and the structure of the grains in each zone can be observed. The fusion zone is composed of coarse columnar dendrites governed by the G/R ratio, known as constitutional supercooling. Namely, it has been known that the greater the degree of constitutional supercooling, the greater the tendency for a given material to switch from the cellular to the dendritic mode of solidifiaction. Again, the bead at 45° is unique in that it has the coarsest grains in the melted zone. Its grains are very coarse columnar grains. Thus, it can be concluded that in the case of the weld bead at 45°, the columnar growth in the direction of the maximum temperature gradient dominates over the grain's preferred direction of growth, the easy growth direction and that the cooling rate in this region was the highest. Besides the epitaxial growth of the original grain boundaries, there exists a large number of fine columnar subgrain boundaries that are also rich in the precipitates. At 270°, columnar grains are still dominant but their length is visibly smaller, and they are wider. Since at this angle more material exists around the bead, the grain growth does not only occur against vertical heat flow. In this case, another type of columnar grain known as the axial grain exists in the fusion zone. Most of these columnar grains initiate in the original weld bead and continue

Table 2
Nominal chemical composition of the iron-carbon used in this investigation

Component wt. %	C	Fe	Mn	P	S
AISI 1018	0.14–0.2	98.81–99.26	0.6–0.9	Max 0.04	Max 0.05

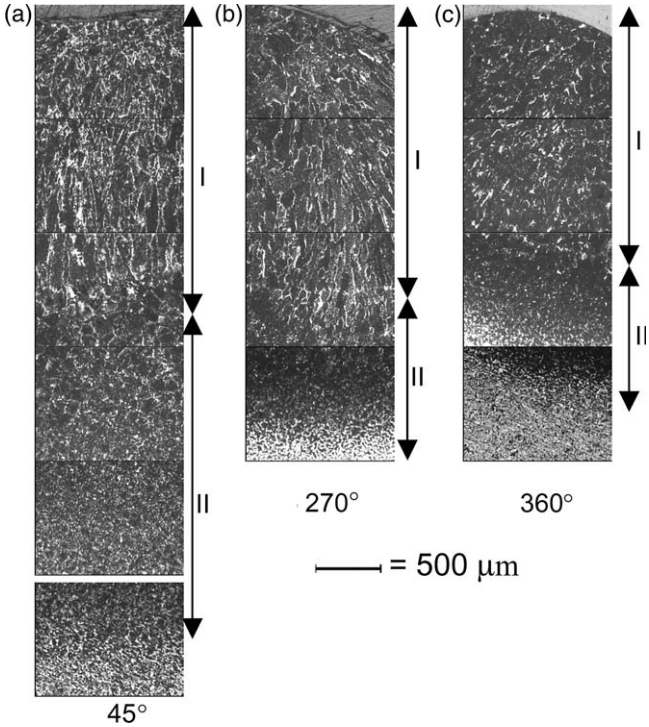

Fig. 10. Enlarged beads at different angles.

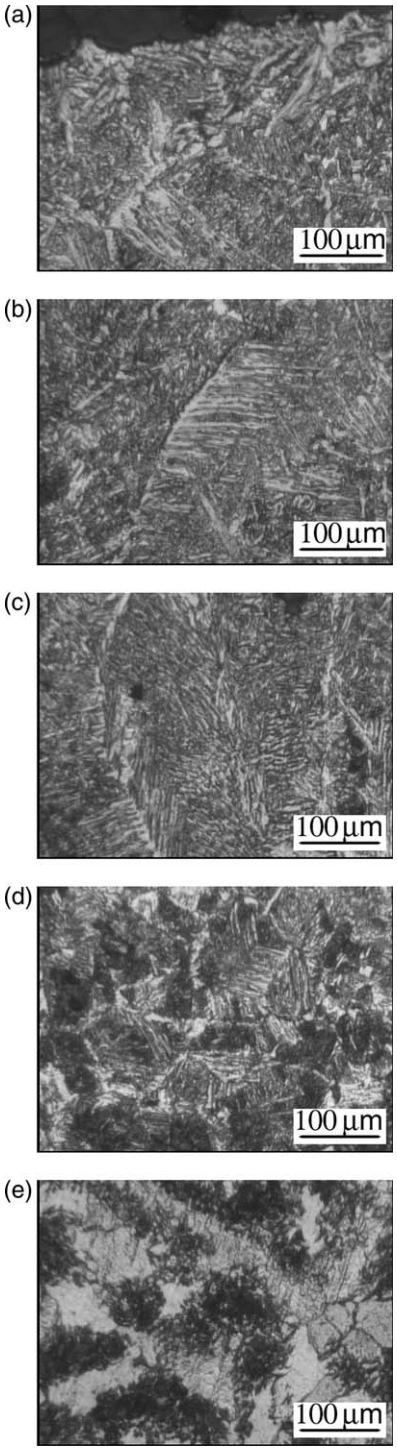

Fig. 11. 45°.

along the length of the weld, blocking the columnar grains growing in from the fusion lines. In this case, this competitive growth between columnar growth, grain axial growth, and grain growth in its own preferred direction dictates the fusion-zone microstructure. At 360°, heat is conducted in all directions, and as a result, very fine columnar grains are formed. Therefore,

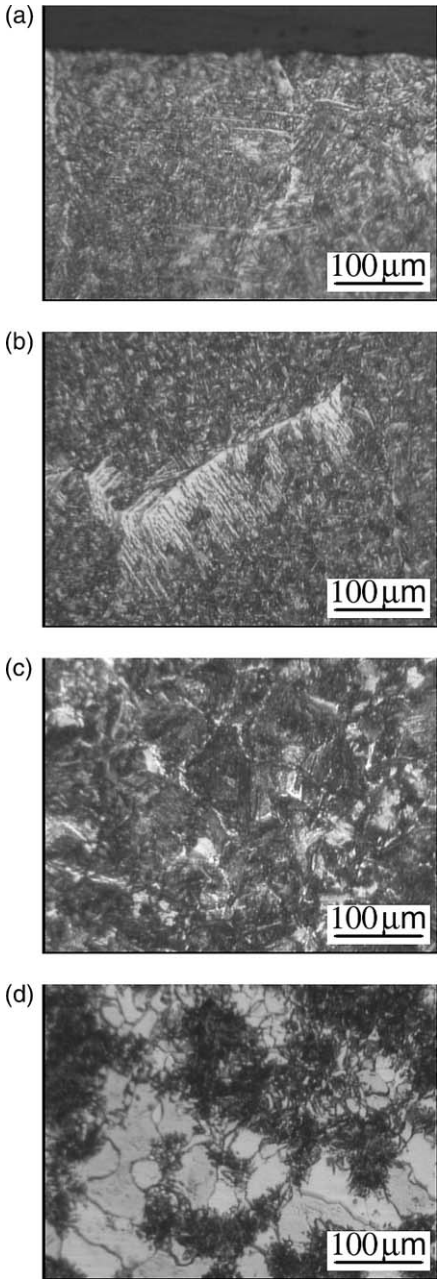

Fig. 12. 270°.

in this case, the grain growth in a preferred direction and the axial grain growth dominate over the columnar grain in the direction of the maximum temperature gradient. In addition, the change in the solidification morphology could have also been due to the differences in thermal and fluid conditions in the filler-deposited molten pool. It should be noted that all three deposited beads exhibit equiaxed grains at the top part of the bead. The influence of the volume of the heat sink is clear. Not only is it true that with the smaller heat sink the temperature rises and more material is melted resulting in a larger heat-affected zone, but it is also

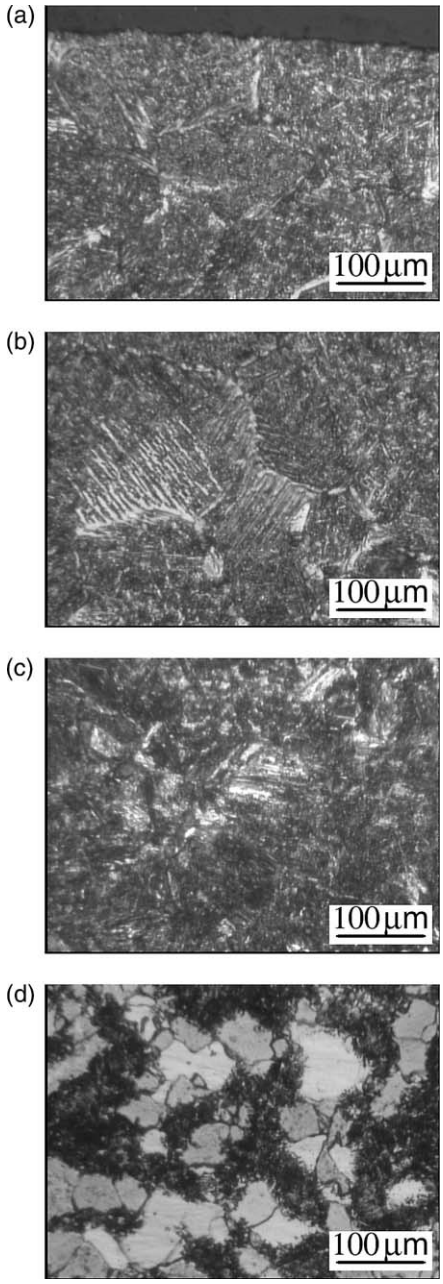

Fig. 13. 360°.

true that the material properties are different as well. This difference means that the physical properties will not be uniform if the process parameters are constant regardless of the geometry.

As it is already mentioned, all three beads consist of the build-up zone, the penetration zone, and the heat-affected zone. The build-up zone and the penetration zone originate from the molten material. Clearly, from knowing the type of the material, it is known that hypoeutectoid compositions will be achieved. Further, which phase constituents will be developed during solidification depend on the cooling rate.

Although the grain size shown in the figures is much different, the phase constituents at different angles are similar. Figs. 11–13 show the typical microstructures in the weld metal of low-carbon, low alloy steels: the grain boundary ferrite, side-plate ferrite, acicular ferrite, pearlite, and martensite. Some fine cementite precipitate at the grain boundaries along a certain crystal plane can be seen in Fig. 11b–13b. The microstructure on the polished-and-etched samples resembles feathers where the spine lies along the prior boundary, and the quills project at oblique angles away from the boundary. The segregation of carbon atoms at the grain boundaries leads to the precipitation of carbides that may distinctly affect the mechanical properties of the beads. Namely, it is well known that the formation of either grain boundary ferrite or ferrite side plates is detrimental to weld metal toughness, since these microstructures provide easy crack propagation paths [19]. In our case, however, the dominant phase is acicular ferrite, which is the one responsible for the high toughness of the weld metal. Acicular ferrite is formed intragranularly, resulting in randomly oriented, short ferrite needles with a basket-weave feature. This interlocking nature, together with its fine grain size, provides the maximum resistance to crack propagation. In our experiment, it should also be noted that the presence of acicular ferrite increases with an increase in the volume of heat sink; and vice versa, at smaller volumes of heat sink, the proportion of grain boundary ferrite and ferrite side plates increases at the expense of acicular ferrite. These increases are because of the higher cooling rate corresponding to the lower heat input at higher angles, and a slower cooling rate owing to the higher heat input at smaller angles.

The heat-affected zone exhibits a fine martensite and α-ferrite microstructure. Again, this microstructure is a direct consequence of the cooling rate since the amount of martensite that is formed increases as the temperature decreases. As it can be seen in Figs. 11b–13b, the martensite grains take on a platelike or needlelike appearance. The white phase in the micrograph could be austenite that did not transform during the rapid cooling or α-ferrite.

3.3. Microhardness analysis

Micro-hardness is an important mechanical property of the materials, which is a measure of a material's resistance to localized plastic deformation, e.g. a small dent or a scratch. A microhardness measurement provides a relatively simple means for determining mechanical properties of small samples. Here, a Vickers micro-hardness testing with a square-based pyramid is used. The hardness, HV, which is equivalent to the indentation pressure, is a function of the applied force,

P, in Newtons and the area of the plastic impression in mm^2 ($H_V = (2P \sin(\theta/2))/d^2$).

It is known that the obtained micro-hardness measurement results depend on many factors, and for this application the most prominent are the used process parameters and the location within the deposited sample. Micro-hardness from the samples obtained from the second experiment is measured. As aforementioned in these experiments, the material is deposited in layers under the different welding parameters. Micro-hardness is measured on one, two, and three deposited layers. The micro-hardness is found to be changeable in the equiaxed, columnar grain regions, and the HAZ of the substrate. In general in all measurements, the deposited layer (or layers) featured by the equiaxed grains on the top of the bead exhibits a higher hardness than the rest of the welding bead that exhibits a columnar grain region and the HAZ of the substrate. All measuring results are obtained from at least three hardness measurements, which are then averaged. Distances

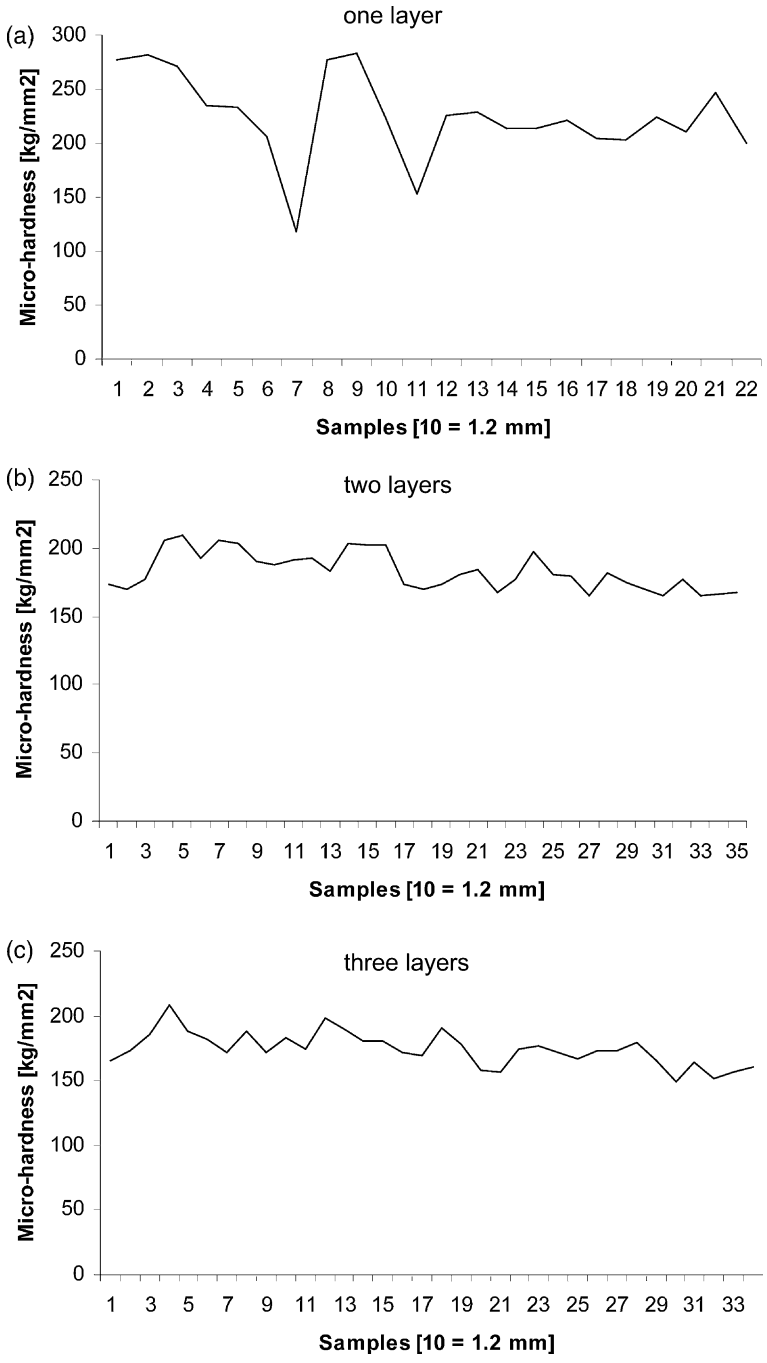

Fig. 14. Microhardness of deposited layers.

between two measurements are 120 μm, and measurements start from the top of the bead towards the substrate.

The results show that the material at the top of the welding bead is hardest and becomes softer and softer as measurements are taken toward the substrate. In addition, the hardest material is obtained from the equiaxed top area of samples with one layer. The highest obtained value for this sample is 280 kg/mm^2. Samples with two and three layers exhibit a softer material in the lower layers, whose value is in the range of 150–180 kg/mm^2. This softening is expected since adding new layers reheats already deposited material which, consequently, softens slightly. Thus, adding every new layer makes previous layers slightly softer. This influence of the reheating is smaller and smaller with the addition of more layers. These results could be seen from Fig. 14a–c, where the hardness for the samples obtained with a current of 120 A, and a wire-feeding speed of 40 cm/min are shown. In this figure, the horizontal axis represents a number of the sample where the first measurement is taken close to the top of the welding bead, and the others are taken in equal steps toward the end of the HAZ. First, it should be noted that the average hardness values decrease going from the top of the bead toward the HAZ. Second, measurements of the hardness of the deposits that consist of more then one layer exhibit lower values, which is a consequence of the already mentioned reheating of the welding beads.

After microstructural and micro-hardness analyses, the quantitative analyses of the microstructures of the same specimens were performed. As it is well known, the microstructure composition is mostly affected by the chemical composition and by the cooling rate. Therefore, the combination of pearlite, ferrite, bainite, and martensite exist in a microstructure as the result of the cooling transformations. Moreover, their morphologies differ with the different temperature achieved (higher temperatures closer to the top surface that is directly exposed to the arc) and with the different cooling rates. However, the quantitative analysis is performed by using the optical microscope, and as a result, on several occasions, it was difficult to distinct microstructure composition, especially between the ferrite side plates and bainitic ferrite. Analysis showed that observed samples consist of ferrite and bainite ~66%, perlite ~32%, and martensite ~2%, which is in very good agreement with the data found in the literature [20,21], where similar results are expected for the cooling time of ~200 s (cooling time from Ac_3 to 773 K). For this cooling rate, from the literature [20,21] it is expected that the material should have micro-hardness of 150–160 kg/mm^2. It should be noticed that the results from the experiments in general exhibit higher micro-hardness values, which may be due to the slightly higher percentage of martensite.

4. Conclusions

A microstructure of the 3D parts, built by RP based on deposition by GTA welding is examined. Material used for building 3D parts is AISI 1018. A new experimental setup is developed which consists of a six-axis robot, a CNC machine, a wire-feeding mechanism, a torch, and a welding power supply. Two sets of experiments are carried out. In the first experiment, since the final microstructure of the steel depends upon its composition and the thermo-mechanical history, the temperature at the locations with different heat-transfer conditions are monitored by thermocouples. The relationships between the geometry of the deposited beads and the welding parameters are developed. The microstructure analysis of fusion and the heat-affected zone is performed. Different heat-transfer conditions cause different cooling rates and, consequently, different microstructures. Thus, all the deposited beads exhibit equiaxed dendrites at the top layer, but different grain sizes within the bead with different conditions. The best microstructure is achieved with samples that have the most uniform heat-transfer conditions at 360° angle. Samples from the second experiment are examined on Vickers micro-hardness tests. The results from all samples showed that layers possess a maximum micro-hardness at the top deposited layer, while there is a slight decreasing trend towards the middle and the bottom layers. Both experiments proved that 3D parts built in this manner have a uniform microstructure, and there is no porosity or cracks. It is shown that the volume of heat sink plays a very important roll in the creation of the microstructure and mechanical properties of the deposited beads. The obtained results show that RP based on GTA welding can be successfully used for building 3D parts. In order to further improve the quality of deposited layers, it is necessary to adjust the heat input according to the volume of the heat sink, so that the same maximum temperature is achieved across the layers. This goal will be challenging in a subsequent research.

Acknowledgements

This work was financially supported by THECB Grant 003613-0016-2001, NSF Grant No. DMI-9232848, and the US Department of Education Grant No. P200A80806-98. Assistance by Mr. M. Valant during the experiments is gratefully acknowledged.

References

[1] I. Kmecko, D. Hu, R. Kovacevic, Controlling heat input, spatter and weld penetration in GMA welding for solid freeform fabrication, Proceedings of the 10th Solid Freeform Fabrication, Symposium, August, Austin, 1999.

[2] R. Kovacevic, Rapid manufacturing of functional parts based on deposition by welding and 3D laser cladding, Proc MoldMaking Conference, April 3–5, Rosemont, IL, presented by the MoldMaking Technology Magazin, 2001, pp. 253–276.

[3] Z. Jandric, I. Kmecko, R. Kovacevic, Dynamic modeling of GTAW for rapid prototyping with welding-based deposition, in: T.A. Siewert (Ed.), 11th International Conference on Computer Technology in Welding, December 3–5, Columbus, OH, NIST Special Publication 973, 2001.

[4] J.D. Spencer, P.M. Dickens, C.M. Wykes, Rapid prototyping of metal parts by three-dimensional welding, ImechE Proc Part B, J. Eng. Manufact. 212 (1998) 175–182.

[5] P. Dickens, R. Cobb, I. Gibbson, M. Pridham, Rapid prototyping using 3D welding, J. Design. Manufact. 3 (March, 1) (1993) 39–44.

[6] R. Merz, F. Prinz, K. Ramaswami, M. Terk, L. Weiss, Shape deposition manufacturing, Proceeding of the Solid Freeform Fabrication Symposium, University of Texas, Austin, Texas, August 8–10, 1994.

[7] K. Karunakaran, P. Shanmuganathan, S. Roth-Koch, K. Koch, Direct rapid prototyping tools, Proceedings of the Solid Freeform Fabrication, Symposium, University of Texas, Austin, 1998, pp. 105–112.

[8] A. Ribero, J. Norrish, Rapid prototyping process using metal directly, Proceedings of Solid Freeform Fabrication, Symposium, 12–14 August, Austin, 1996, pp. 249–256, ISSN 1053-2153.

[9] T.E. Doyle, D.P. Edmonds, M.D. McAninch, P.M. Ryan, Method and apparatus for building a workpiece by deposit welding, US Patent No. 4,842,186 (1989).

[10] C.L. Buhrmaster, D.E. Clark, H.B. Smartt, Apparatus for gas-metal arc deposition, US Patent No. 5,052,331 (1991).

[11] F.B. Prinz, L.E. Weiss, Method and apparatus for fabrication of three-dimensional metal articles by weld deposition, US Patent No. 5,207,371 (1993).

[12] S. Aleshin, Method for depositing material on the tip of a gas turbine engine airfoil using linear translational welding, US Patent No. 5,160,822 (1992).

[13] F. Schneebeli, O. Braun, B. Tanner, R. Dekumbis, Method of production of workpieces by welding equipment, US Patent No. 5,233,150 (1993).

[14] K. Kassmaul, F.W. Schoch, H. Lucknow, High quality large components "shape welded" by a SAW process, Welding Journal 62 (9) (1983) 17–24.

[15] S. Yang, M. Han, Q. Wang, Development of a welding system for 3D steel rapid prototyping process, China Welding 10 (1) (2001) 50–56, English edition.

[16] Z. Jandric, J.H. Ouyang, R. Kovacevic, Effect of volume of heat sink on process and physical properties of parts built by welding based SFF, 13th Annual Solid Freeform Fabrication Symposium, August, 5–7, Austin, 2002.

[17] R. Kovacevic, Z. Jandric, H. Wang, Development of welding-based layered manufacturing/repair process, 55th Annual Assembly of the International Institute of Welding Commission IV Meeting—High Energy Beam Welding, June, Copenhagen, Denmark, 2002.

[18] Z. Jandric, Y.Z. Wang, R. Kovacevic, Optimization of welding parameters for GTAW based rapid manufacturing, 6th International Conference on Trends in Welding, April 15–19, Pine Mountain, Georgia, 2002.

[19] W.D. Callister, Material Science and Engineering—An Introduction, 4th edn, John Wiley & Sons, USA, 1996, ISBN 0-471-13459-7.

[20] M. Bauccio, ASM Metals Reference Book, 3rd ed., ASM International, 1993.

[21] C.J. Smithells, Metals Reference Book, 7th ed., Butterworth-Heinemann, Oxford, Boston, 1998.